Biosensors and Bioelectronics 61 (2014) 386–390

Contents lists available at ScienceDirect

Biosensors and Bioelectronics

journal homepage: www.elsevier.com/locate/bios

Short communication

"Chemical nose" for the visual identification of emerging ocular pathogens using gold nanostars

Mohit S. Verma [a,b,1], Paul Z. Chen [a,1], Lyndon Jones [a,c], Frank X. Gu [a,b,*]

[a] Department of Chemical Engineering, University of Waterloo, 200 University Avenue W, Waterloo, Ontario, Canada N2L 3G1
[b] Waterloo Institute for Nanotechnology, University of Waterloo, 200 University Avenue W, Waterloo, Ontario, Canada N2L 3G1
[c] Center for Contact Lens Research, University of Waterloo, 200 University Avenue W, Waterloo, Ontario, Canada N2L 3G1

ARTICLE INFO

Article history:
Received 26 March 2014
Received in revised form
16 May 2014
Accepted 19 May 2014
Available online 27 May 2014

Keywords:
Color change
Visual detection
Microbial keratitis
Contact lens cases
Gold nanoparticles
Point-of-care

ABSTRACT

Ocular pathogens can cause serious damages in the eye leading to severe vision loss and even blindness if left untreated. Identification of pathogens is crucial for administering the appropriate antibiotics in order to gain effective control over ocular infection. Herein, we report a gold nanostar based "chemical nose" for visually identifying ocular pathogens. Using a spectrophotometer and nanostars of different sizes and degrees of branching, we show that the "chemical nose" is capable of identifying the following clinically relevant ocular pathogens with an accuracy of 99%: *S. aureus*, *A. xylosoxidans*, *D. acidovorans* and *S. maltophilia*. The differential colorimetric response is due to electrostatic aggregation of cationic gold nanostars around bacteria without the use of biomolecule ligands such as aptamers or antibodies. Transmission electron microscopy confirms that the number of gold nanostars aggregated around each bacterium correlates closely with the colorimetric response. Thus, gold nanostars serve as a promising platform for rapid visual identification of ocular pathogens with application in point-of-care diagnostics.

1. Introduction

Microbial keratitis poses a great risk for vision loss (Bertino, 2009). Contact lenses are the most common risk factor that predispose wearers to keratitis (Tilia et al., 2014; Stapleton and Carnt, 2012; Bui et al., 2010; Hall and Jones, 2010; Green et al., 2008; Keay et al., 2006; de Oliveira et al., 2003). The fundamental challenge in mitigating keratitis is detecting these pathogens early and more importantly, identifying the species for designing a more effective treatment regimen (Mascarenhas et al., 2014; Inoue and Ohashi, 2013; Hau et al., 2010). The current gold standard for identifying the pathogens relies on microbial cultures or genomic analysis, which must be done in a central laboratory (Taravati et al., 2013). Recent advances in biosensors offer the potential to perform these tests at the point-of-care (Chan and Gu, 2013; Verdoy et al., 2012). Common approaches employ a colorimetric method (Safavieh et al., 2014; Li et al., 2011) or microelectronics for sensing (Oh et al., 2013; Safavieh et al., 2012; Siddiqui et al., 2012; Pohlmann et al., 2009). A recent study has shown improvement of detection capabilities to allow sub-cellular measurements of individual cells (Kanwal et al., 2013). However, a major challenge remains to be solved: identifying species of bacteria at the point-of-care, which is crucial because of growing antibiotic resistance (Bertino, 2009) and unique drug susceptibility profiles of pathogens (Jacquier et al., 2012). Lately, the prevalence of Gram-negative *Achromobacter* (Park et al., 2012; Ahmed and Pineda, 2011; Kiernan et al., 2009), *Stenotrophomonas* (Dantam et al., 2011) and *Delftia* (Ray and Lim, 2013) has been emphasized because of their innate ability to form biofilms in contact lenses and their accompanying cases. Moreover, these pathogens present an increasing problem due to their capability to survive in contact lens care solutions (Wiley et al., 2012) and cause microbial keratitis (Hall and Jones, 2010). Hence, there exists a need for a platform that rapidly identifies multiple pathogens affecting contact lens wearers.

Gold nanoparticles have been used extensively as colorimetric biosensors due to their high absorption coefficients, enhanced scattering, unique localized surface plasmon resonance and high surface area to volume ratio (Azzazy et al., 2012; Li et al., 2012; Chen et al., 2010). The optical properties of gold nanoparticles can be further exploited by varying their shape, size and surface characteristics. Gold nanostars are an interesting class of nanoparticles; their optical properties can be fine-tuned by altering the size and degree of branching (Verma et al., 2014; Shao et al., 2012; Kumar et al., 2008). Nanostars coated with specific antibodies have demonstrated the colorimetric detection of a single species of

* Corresponding author at: Department of Chemical Engineering, University of Waterloo, 200 University Avenue W, Waterloo, Ontario, Canada N2L 3G1.
Tel.: +1 519 888 4567x38605; fax: +1 519 888 4347.
E-mail address: frank.gu@uwaterloo.ca (F.X. Gu).
[1] Authors contributed equally.

http://dx.doi.org/10.1016/j.bios.2014.05.045
0956-5663/

bacteria (Khan et al., 2011), but a ubiquitous platform for the colorimetric detection and identification of bacteria is rare. A small body of work is present on the use of cationic nanoparticles coupled with fluorescent polymers for identification of bacteria using a "chemical nose" approach, where a unique set of responses is obtained for each species of pathogen (Wan et al., 2014; Phillips et al., 2008). The existing methods require the modification of gold nanoparticles with multiple ligands and the use of a fluorescent spectrometer, which is not easily accessible in a point-of-care setting. In our recent work, a library of gold nanostars was developed with tunable color change in the presence of *S. aureus* (Verma et al., 2014). Here, we show that gold nanostars can be used as a "chemical nose" not only for detecting bacteria but also for identifying their species without the use of antibodies or aptamers. The specificity of the "chemical nose" is a result of the ability of cationic gold nanostars to electrostatically aggregate around bacteria and provide a colorimetric response based on intrinsic physicochemical differences between bacteria, such as surface charge, surface area and morphology (Verma et al., 2014).

2. Materials and methods

2.1. Materials

Details about the materials used have been presented in Supplementary material Section S1.1.

2.2. Synthesis of gold nanostars

The gold nanostars were synthesized by modifying a previously described procedure (Verma et al., 2014; Lu et al., 2010). Detailed modifications are included in Section S1.2 of Supplementary material.

2.3. Bacterial culture

Staphylococcus aureus, *Achromobacter xylosoxidans*, *Delftia acidovorans* and *Stenotrophomonas maltophilia* were used for detection and identification experiments. The details about culturing are included in Section S1.3 of Supplementary material. When bacteria are added to gold nanostars, a final absorbance at 660 nm (OD_{660}) of 0.02 is expected for the bacteria.

2.4. Identification of bacterial species

Detailed procedure of the identification assay is included in Section S1.4 of Supplementary material. After obtaining the absorption spectra, the normalized absorbance values were obtained for all samples by using the following equation:

$$\begin{aligned}&\text{Normalized absorbance}\\&=(\text{average saline control absorbance at }\lambda\\&-\text{average saline control absorbance at 800 nm})\\&-(\text{sample absorbance at }\lambda-\text{sample absorbance at 800 nm})\end{aligned}$$

where λ is the wavelength of particular importance: 583 nm peak for blue nanostars, 541 nm peak for red nanostars and 544 nm peak and 583 nm for purple nanostars. The absorbance at 800 nm was used as the baseline. The data was then subjected to a classical linear discriminant analysis (LDA) using MySTAT (version 12.02) where each population in the training set was assigned a numerical identifier and this identifier was used as the grouping variable while the normalized absorbance values from the purple nanostars were used as the two predictors. Classification of unknown samples was performed by determining the shortest Mahalanobis distance to the groups generated using the training matrix. During the identification of unknown bacteria samples, the experiment preparation and data collection were performed by two different researchers resulting in a blinded process.

2.5. Transmission electron microscopy of bacteria and gold nanostars

Detailed procedure of obtaining transmission electron microscopy (TEM) images is outlined in Section S1.5 of Supplementary material.

3. Results and discussion

3.1. Visual color change with gold nanostars

In order to develop a "chemical nose," we need various gold nanoparticles that can interact with bacteria to provide a specific response. We hypothesize that if gold nanostars with different sizes and degrees of branching are incubated with a particular species of bacteria, each nanostar will provide a unique colorimetric response. To test this hypothesis, we chose the commonly occurring Gram-positive *S. aureus* and Gram-negative ocular pathogens *A. xylosoxidans*, *D. acidovorans* and *S. maltophilia* as the pathogens of interest (Kilvington et al., 2013) and added them to gold nanostars to obtain a drastic colorimetric response. Two types of nanostars were synthesized such that there would be distinct differences in color (blue and red), size and degree of branching. Thus, each nanostar solution should interact differently between species of bacteria depending on a species' surface charge, surface area and morphology to provide a "chemical nose" sensor. The blue nanostars have a greater size and higher degree of branching (Fig. 1a) as compared to the red nanostars, which are smaller and more spherical in shape (Fig. 1b). These two nanostar solutions were also mixed by 1:1 volume to obtain a third solution of purple nanostars in order to investigate the co-operative response from the two nanoparticles. The three nanostar solutions were added to adjacent microplate wells and mixed with saline with nutrient broth (as control) and different species of bacteria at the same optical density. A sample image is presented in Fig. 1c, where the bacterial species are visually discernible. Amongst these species, *S. aureus* and *S. maltophilia* present the most striking differences as compared to saline. In the case of *S. aureus*, the gold nanostar solutions have a tinge of their respective original color whereas for *S. maltophilia*, the samples lose their original color to nearly clear. This suggests a more complete aggregation of gold nanostars in the presence of *S. maltophilia* as compared to other species of bacteria. *D. acidovorans* and *A. xylosoxidans* produce a lower degree of color change. In the case of *D. acidovorans*, a color change of the red nanostars is seen to a slight purple, which is unique in comparison to other species. Thus, the red nanostars show a more drastic color change as compared to blue nanostars which allows for visual distinction between *A. xylosoxidans* and *D. acidovorans*. The purple nanostar solution behaves similar to blue stars in the case of *S. aureus* but it appears to be a superposition of blue and red nanostar responses in the presence of all other species of bacteria.

3.2. Colorimetric identification of bacteria

The absorption spectra of each gold nanostar solution in the presence of bacteria are presented in Fig. 2a–c. The observations from the spectra are consistent with the visual observations where *S. maltophilia* shows the most drastic change in spectra. In the case of blue nanostars, the peak with *S. maltophilia* is almost flattened whereas for red nanostars, there is partial flattening. The purple

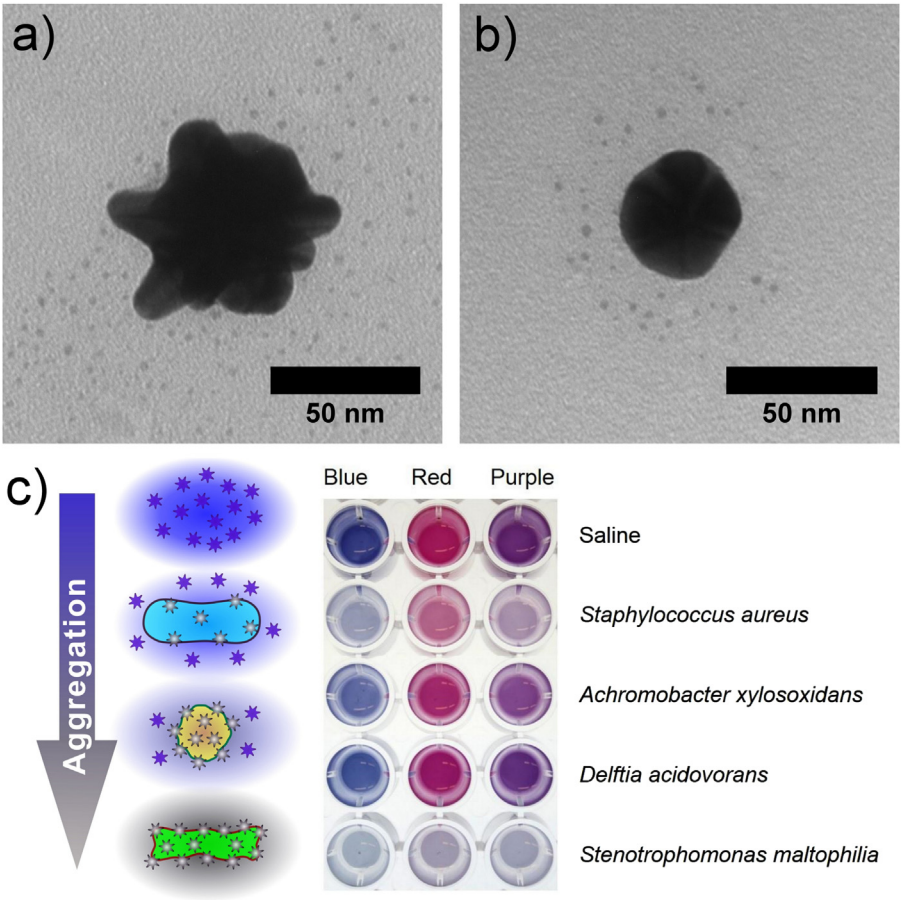

Fig. 1. Transmission electron microscopy images of (a) branched blue gold nanostar and (b) spherical red gold nanostar. (c) Change in color of gold nanostars caused by varying degrees of aggregation due to the differences in surface charge, surface area and morphology of bacteria. The photograph shows the color when species of bacteria with final $OD_{660}=0.02$ are added to different gold nanostars. (For interpretation of the references to color in this figure legend, the reader is referred to the web version of this article.)

nanostar responses appear to be a linear combination of blue and red nanostars. In the case of *D. acidovorans*, while the absorbance peak does not drop significantly for red and purple nanostars, a red shift and drop is observed for blue nanostars (Fig. 2a). In all other bacterial species, the location of absorbance peak remains consistent but the absorbance values are reduced. Each gold nanostar solution has a unique absorption peak, which resembles the localized surface plasmon resonance wavelength. As shown in Fig. 2a and b, blue and red nanostars have peaks at 583 nm and 541 nm respectively. Purple nanostars have a peak at 544 nm (close to that of red nanostars); however, the absorbance at 583 nm is also of interest to determine the response characteristics from the blue nanostars constituents. The absorbance at 541 nm of red nanostars constituents was not found to be important since it was close to the natural peak of 544 nm of purple nanostars. The absorbance values from these peaks were obtained and normalized against saline with broth as well as baseline absorbance at 800 nm. These normalized values are presented in Fig. 2d and demonstrate that each species of bacteria interacts in a unique manner with blue, red and purple nanostar solutions. We further analyzed these normalized values to create a training set for the identification of species of bacteria.

Using LDA, we observed that identification of each population of bacteria was possible by using the two normalized absorbance values from purple nanostars (544 nm and 583 nm). This is demonstrated in Fig. 2e, where each species of bacteria as well as saline control is statistically discernable using 95% confidence intervals. Here, factors are a linear combination of the absorbance values from purple nanostars as determined by their respective canonical discriminant functions using MySTAT:

$$\text{Factor (1)} = -28.9 + 154.9 \times \text{Purple}_{544\ \text{nm}} - 101.8 \times \text{Purple}_{583\ \text{nm}}$$

$$\text{Factor (2)} = -3.0 + 325.0 \times \text{Purple}_{544\ \text{nm}} - 443.3 \times \text{Purple}_{583\ \text{nm}}$$

Thus, factor (1) gives a greater weight to the absorbance at 544 nm while factor (2) gives more weight to absorbance at 583 nm but the values from both of these wavelengths are required for discriminating the populations of bacteria since neither coefficients are negligible as compared to the other. This training set was then used to identify unknown samples using MySTAT ($p > 0.95$), and it was demonstrated that 99% (78/79 samples) of the samples could be identified accurately with their respective group. Only one of the samples was incorrectly classified as *S. aureus* when it was supposed to be *A. xylosoxidans*. We are currently investigating this outlier and also developing methods to eliminate misclassification. Overall, these are noteworthy results since only two inputs are being used to identify five different populations of samples. It has been demonstrated that the unique surface charge on different species of bacteria can be utilized for identification when electrostatic interactions are used (Phillips et al., 2008). Previous work required the modification of gold nanoparticles with a variety of molecules to provide unique surface charges and hydrophobicity for enhancing the interaction with bacteria. Additionally, these gold nanoparticles are generally coupled with fluorescent polymers to provide the response and hence require fluorescence spectrometry. In the present study,

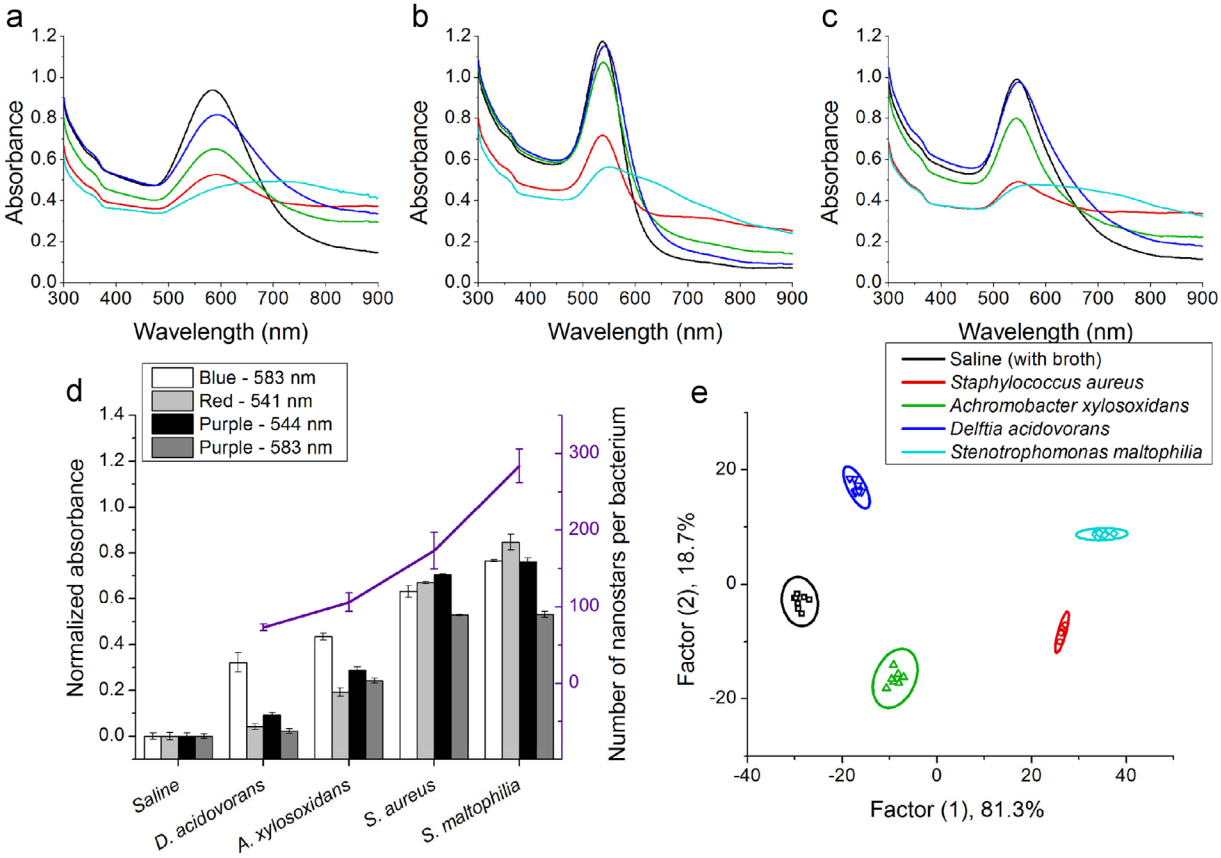

Fig. 2. Response of gold nanostars to saline (with broth) control and different species of bacteria at OD_{660}=0.02. Absorption spectra of (a) blue nanostars; (b) red nanostars; (c) purple nanostars. (d) Normalized absorbance response (n=7–8; mean ± S.D.) and average number of aggregated gold nanostars per bacterium by TEM (n=8; mean ± S.E.). (e) Canonical scores plot of the response from LDA of purple nanostars (544 nm and 583 nm) for different species of bacteria. 95% confidence ellipses are presented for each population. (For interpretation of the references to color in this figure legend, the reader is referred to the web version of this article.)

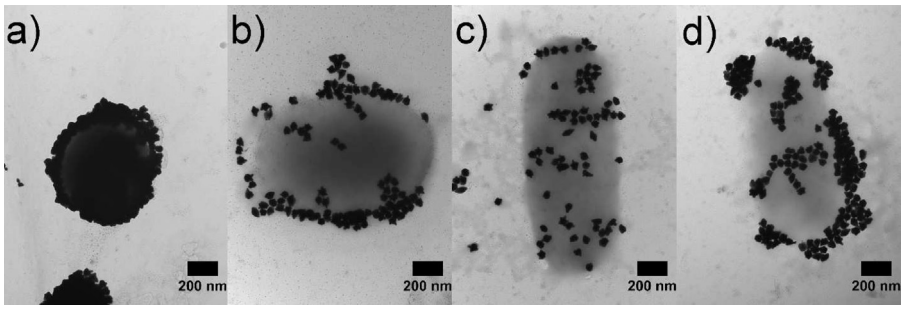

Fig. 3. TEM images of blue gold nanostars aggregating around bacteria: (a) *Staphylococcus aureus*, (b) *Achromobacter xylosoxidans*, (c) *Delftia acidovorans*, (d) *Stenotrophomonas maltophilia*. Scale bars are 200 nm each.

identifying bacterial species was possible visually as well as spectrophotometrically. We exploit the inherent properties of gold nanostars rather than modifying them with specific surface ligands. The cetyltrimethylammonium bromide (CTAB) surfactant of gold nanostars is present on as-synthesized nanoparticles and serves as the source of positive surface charge. We have shown previously that the CTAB-coated nanostars (zeta potential of +38.0 mV) require a polyanionic surface for aggregation and color change (Verma et al., 2014). Such a polyanionic surface is provided in Gram-positive bacteria by teichoic acids (Berry and Saraf, 2005; Berry et al., 2005) and in Gram-negative bacteria by lipopolysaccharides and phospholipids (Sun et al., 2012; Hong and Brown, 2006). The intrinsically different distribution of charges on the surface of bacteria caused by the composition of proteins, polysaccharides and lipids (Boonaert and Rouxhet, 2000; Navarre and Schneewind, 1999; DiRienzo et al., 1978) is responsible for causing the unique electrostatic interactions with gold nanostars. This unique surface composition can be considered to be a fingerprint of the bacteria and probed using the gold nanostars to obtain a colorimetric response. It is expected that gold nanostars with significant protruding branches will interact more strongly with the surface of bacteria due to higher effective surface area and spatial extent as compared to more spherical nanostars (Verma et al., 2014). These inherent differences in branching and size provide different colorimetric outputs since their localized surface plasmon resonance is sensitive to the degree of aggregation (Xia et al., 2010).

3.3. Transmission electron microscopy imaging of bacteria

We used TEM to confirm that the gold nanostars were aggregating around the bacteria of interest (Fig. 3). It was observed that gold nanostars aggregate around bacteria with different shapes (spherical or rod-like) as well as types (Gram-positive or Gram-negative). The TEM samples were rinsed with Millipore water once before drying to remove excess gold nanostars and assist in visualization. Since gold nanostars remained on the bacteria even after rinsing, the images suggest a strong electrostatic interaction, which governs the degree of aggregation and hence the colorimetric response provided by the gold nanostars. This is shown in Fig. 2d since a close correlation is observed between the number of blue gold nanostars aggregated per bacterium and the normalized absorbance observed for the blue nanostars. Further discussion of the TEM images is found in Supplementary material Section S2.1. The simplicity and rapid response of the assay gives the potential of implementation in a consumer product or at the point-of-care.

4. Conclusion

We demonstrated that gold nanostars are a versatile platform for identifying species of bacteria such as *S. aureus*, *A. xylosoxidans*, *D. acidovorans* and *S. maltophilia*, where all the species were visually discernible and 99% of the samples were identified correctly using a spectrophotometer and LDA. The use of two different CTAB-coated gold nanostars provided unique colorimetric outputs corresponding to the dependence of electrostatic interactions on size and shape of nanostars and surface characteristics of bacteria. TEM was used to show a correlation in the degree of aggregation and the colorimetric response of gold nanostars in the presence of both Gram-positive and Gram-negative bacteria. Thus, CTAB-coated gold nanostars are a promising “chemical nose” platform for simple visual identification of bacterial contaminants for point-of-care diagnostics.

Acknowledgments

This work was financially supported by the Natural Sciences and Engineering Research Council of Canada (NSERC) and 20/20: NSERC – Ophthalmic Materials Network. M. S. Verma is grateful for the NSERC Vanier Canada Graduate Scholarship. P. Z. Chen is thankful for the NSERC Undergraduate Student Research Award.

Appendix A. Supplementary material

Supplementary data associated with this article can be found in the online version at http://dx.doi.org/10.1016/j.bios.2014.05.009.

References

Ahmed, A.A., Pineda, R., 2011. Eye Contact Lens 37, 386–389.
Azzazy, H.M., Mansour, M.M., Samir, T.M., Franco, R., 2012. Clin. Chem. Lab. Med. 50, 193–209.
Berry, V., Gole, A., Kundu, S., Murphy, C.J., Saraf, R.F., 2005. J. Am. Chem. Soc. 127, 17600–17601.
Berry, V., Saraf, R.F., 2005. Angew. Chem. Int. Ed 44, 6668–6673.
Bertino Jr., J.S., 2009. Clin. Ophthalmol. 3, 507–521.
Boonaert, C.J., Rouxhet, P.G., 2000. Appl. Environ. Microbiol. 66, 2548–2554.
Bui, T.H., Cavanagh, H.D., Robertson, D.M., 2010. Eye Contact Lens 36, 334–339.
Chan, T., Gu, F., 2013. Biosens. Bioelectron. 42, 12–16.
Chen, C., Zhao, C., Yang, X., Ren, J., Qu, X., 2010. Adv Mater. 22, 389–393.
Dantam, J., Zhu, H., Stapleton, F., 2011. Investig. Ophthalmol. Vis. Sci. 52, 51–57.
de Oliveira, P.R., Temporini-Nastari, E.R., Ruiz Alves, M., Kara-Jose, N., 2003. Eye Contact Lens 29, 164–167.
DiRienzo, J.M., Nakamura, K., Inouye, M., 1978. Annu. Rev. Biochem. 47, 481–532.
Green, M., Apel, A., Stapleton, F., 2008. Cornea 27, 33–39.
Hall, B.J., Jones, L., 2010. Eye Contact Lens 36, 101–105.
Hau, S.C., Dart, J.K., Vesaluoma, M., Parmar, D.N., Claerhout, I., Bibi, K., Larkin, D.F., 2010. Br. J. Ophthalmol. 94, 982–987.
Hong, Y., Brown, D.G., 2006. Colloids Surf. B Biointerfaces 50, 112–119.
Inoue, T., Ohashi, Y., 2013. Cornea 32 (Suppl. 1), S71–S76.
Jacquier, H., Le Monnier, A., Carbonnelle, E., Corvec, S., Illiaquer, M., Bille, E., Zahar, J.R., Jaureguy, F., Fihman, V., Tankovic, J., Cattoir, V., 2012. Gmc Study Group, 2012. Microb. Drug Resist. 18, 396–401.
Kanwal, A., Lakshmanan, S., Bendiganavale, A., Bot, C.T., Patlolla, A., Raj, R., Prodan, C., Iqbal, Z., Thomas, G.A., Farrow, R.C., 2013. Biosens. Bioelectron. 45, 267–273.
Keay, L., Edwards, K., Naduvilath, T., Taylor, H.R., Snibson, G.R., Forde, K., Stapleton, F., 2006. Ophthalmology 113, 109–116.
Khan, S.A., Singh, A.K., Senapati, D., Fan, Z., Ray, P.C., 2011. Chem. Commun. 47, 9444–9446.
Kiernan, D.F., Chin, E.K., Sclafani, L.A., Saidel, M.A., 2009. Eye Contact Lens 35, 212–214.
Kilvington, S., Shovlin, J., Nikolic, M., 2013. Cont Lens Anterior Eye 36, 294–298.
Kumar, P.S., Pastoriza-Santos, I., Rodriguez-Gonzalez, B., de Abajo, F.J.G., Liz-Marzan, L.M., 2008. Nanotechnology 19, 015606.
Li, C.Z., Vandenberg, K., Prabhulkar, S., Zhu, X., Schneper, L., Methee, K., Rosser, C.J., Almeide, E., 2011. Biosens. Bioelectron. 26, 4342–4348.
Li, W., Feng, L., Ren, J., Wu, L., Qu, X., 2012. Chemistry 18, 12637–12642.
Lu, W., Singh, A.K., Khan, S.A., Senapati, D., Yu, H., Ray, P.C., 2010. J. Am. Chem. Soc. 132, 18103–18114.
Mascarenhas, J., Lalitha, P., Prajna, N.V., Srinivasan, M., Das, M., D'Silva, S.S., Oldenburg, C.E., Borkar, D.S., Esterberg, E.J., Lietman, T.M., Keenan, J.D., 2014. Am. J. Ophthalmol. 157, 56–62.
Navarre, W.W., Schneewind, O.s, 1999. Microbiol. Mol. Biol. Rev. 63, 174–229.
Oh, S., Jadhav, M., Lim, J., Reddy, V., Kim, C., 2013. Biosens. Bioelectron. 41, 758–763.
Park, J.H., Song, N.H., Koh, J.W., 2012. Korean J. Ophthalmol. 26, 49–53.
Phillips, R.L., Miranda, O.R., You, C.C., Rotello, V.M., Bunz, U.H., 2008. Angew. Chem. Int. Ed 47, 2590–2594.
Pohlmann, C., Wang, Y., Humenik, M., Heidenreich, B., Gareis, M., Sprinzl, M., 2009. Biosens. Bioelectron. 24, 2766–2771.
Ray, M., Lim, D.K., 2013. Eye Contact Lens 39, 192–193.
Safavieh, M., Ahmed, M.U., Sokullu, E., Ng, A., Braescu, L., Zourob, M., 2014. Analyst 139, 482–487.
Safavieh, M., Ahmed, M.U., Tolba, M., Zourob, M., 2012. Biosens. Bioelectron. 31, 523–528.
Shao, L., Susha, A.S., Cheung, L.S., Sau, T.K., Rogach, A.L., Wang, J., 2012. Langmuir 28, 8979–8984.
Siddiqui, S., Dai, Z., Stavis, C.J., Zeng, H., Moldovan, N., Hamers, R.J., Carlisle, J.A., Arumugam, P.U., 2012. Biosens. Bioelectron. 35, 284–290.
Stapleton, F., Carnt, N., 2012. Eye 26, 185–193.
Sun, J., Ge, J., Liu, W., Wang, X., Fan, Z., Zhao, W., Zhang, H., Wang, P., Lee, S., 2012. Nano Res. 5, 486–493.
Taravati, P., Lam, D., Van Gelder, R.N., 2013. Curr. Ophthalmol. Rep. 1 (10) (1007/s40135-013-0025-1).
Tilia, D., Lazon de la Jara, P., Zhu, H., Naduvilath, T.J., Holden, B.A., 2014. Optom. Vis. Sci.
Verdoy, D., Barrenetxea, Z., Berganzo, J., Agirregabiria, M., Ruano-Lopez, J.M., Marimon, J.M., Olabarria, G., 2012. Biosens. Bioelectron. 32, 259–265.
Verma, M.S., Chen, P.Z., Jones, L., Gu, F.X., 2014. RSC Adv. 4, 10660–10668.
Wan, Y., Sun, Y., Qi, P., Wang, P., Zhang, D., 2014. Biosens. Bioelectron. 55, 289–293.
Wiley, L., Bridge, D.R., Wiley, L.A., Odom, J.V., Elliott, T., Olson, J.C., 2012. Investig. Ophthalmol. Vis. Sci. 53, 3896–3905.
Xia, F., Zuo, X., Yang, R., Xiao, Y., Kang, D., Vallee-Belisle, A., Gong, X., Yuen, J.D., Hsu, B.B., Heeger, A.J., Plaxco, K.W., 2010. Proc. Natl. Acad. Sci. USA 107, 10837–10841.